JULY 12 2019

A uniform circular array of isotropic sensors that stochastically dislocate in three dimensions—The hybrid Cramér-Rao bound of direction-of-arrival estimation

Kainam Thomas Wong; Zakayo Ndiku Morris; Dominic Makaa Kitavi; Tsair-Chuan Lin

J. Acoust. Soc. Am. 146, 150–163 (2019)
https://doi.org/10.1121/1.5098771

A uniform circular array of isotropic sensors that stochastically dislocate in three dimensions—The hybrid Cramér-Rao bound of direction-of-arrival estimation

Kainam Thomas Wong,[1] Zakayo Ndiku Morris,[2] Dominic Makaa Kitavi,[3] and Tsair-Chuan Lin[4,a)]

[1]*School of General Engineering, Beihang University*
[2]*Department of Electronic and Information Engineering, Hong Kong Polytechnic University*
[3]*Department of Mathematics, Computing, and Information Technology, University of Embu*
[4]*Department of Statistics, National Taipei University*

(Received 20 November 2018; revised 11 February 2019; accepted 23 March 2019; published online 12 July 2019)

An array's constituent sensors could be spatially dislocated from their nominal positions. This paper investigates how such sensor dislocation would degrade a uniform circular array (UCA) of isotropic sensors (like pressure sensors) in their direction-finding precision. This paper analytically derives this direction finding's hybrid Cramér-Rao bound (HCRB) in a closed form that is expressed explicitly in terms of the sensors' dislocation parameters. In the open literature on UCA direction finding, this paper is the first to be three-dimensional in modeling the sensors' dislocation. Perhaps unexpectedly to some readers, sensor dislocation could improve and not necessarily degrade the HCRB; these opposing effects depend on the dislocation variances, the incident source's arrival angle, and the signal-to-noise power ratio—all analyzed rigorously in this paper. Interesting insights are thereby obtained: (a) The HCRB is *enhanced* for the impinging source's polar arrival angle as the sensors become *more* dislocated *along the impinging wavefront* due to aperture enlargement over the stochastic dislocation's probability space. (b) Likewise, the HCRB is *improved* for the azimuth arrival angle as the sensors become *more* dislocated *on the circular array's plane*, also due to aperture enlargement. (c) In contrast, sensor dislocation *along the incident signal's propagation direction* can only worsen the HRCBs due to nuisance-parameter effects in the Fisher information. (d) Sensor dislocation *orthogonal to the array plane* must degrade the HCRB for the azimuth arrival angle but could improve the HCRB for the polar arrival angle.
 https://doi.org/10.1121/1.5098771

[JFL] Pages: 150–163

I. INTRODUCTION

The circular array (also known as a "ring array") is a popular array configuration; it has been widely implemented and is available as a commercial product. Please see Table I for a partial listing of implemented or commercially available circular arrays of microphones/hydrophones. The circular array is popular partly because its aperture size and beam shape stay effectively constant even as the array's "look direction" varies 360° over the entire azimuth. These advantages stem from the circular geometry's spatial centrosymmetry.

A circular array of uniformly spaced identical isotropic sensors has often been deployed to locate incident emitters' bivariate azimuth-elevation directions-of-arrival: The corresponding Cramér-Rao lower bounds (CRBs) have been much investigated in the research literature. For example,

(i) References 10–16 analytically derive expressions of the CRB in a *closed* form explicitly in terms of the parameters of the statistical data model.
(ii) References 17–27 analytically express the CRB, but in open form (e.g., involving an unsolved integral, an unsolved infinite-term summation, or an unsolved matrix inversion/multiplication) or *implicitly* in terms of the statistical data model parameters.
(iii) References 28–60 plot CRB graphs, but present no mathematical expression of any CRB.

All the above references presume that all sensors are of an ideal gain/phase response, and at the nominal locations.

In the real world, sensors may dislocate randomly from their nominal locations in the array. Such sensor dislocation has never been accounted for in any analytical derivation of the Cramér-Rao bound in the open literature on uniform circular array (UCA) direction finding. That is, the open literature offers no Cramér-Rao bound expression (whether in a closed form or an open form) that incorporates the effects of sensor dislocation. Cramér-Rao bound graphs are only available (*unaccompanied* by any mathematical expression) in Refs. 30, 31, and 33 with sensors limited to only two-dimensional (2D) dislocation on the circle's plane. Instead, this paper will be first in the open literature (to the best of the present authors' knowledge) to *rigorously derive* the Cramér-Rao bound of direction finding using a nominally circular array of identical isotropic sensors that may stochastically dislocate *three*-dimensionally in space.

a)Electronic mail: tsair@mail.ntpu.edu.tw

TABLE I. Practical implementations of a UCA of isotropic sensors.

Number of microphones/ hydrophones	Radius	Reference
4 (Ref. 1)	9 cm	67
6	A choice between 4 cm and 6 cm	2
8 (Ref. 3)	Not stated	4
10	4 cm	5
12	11.9 cm	6
16	8 cm	7
24	5.7 cm	8
32	Not stated	9

The rest of this paper is organized as follows: Section II defines the statistical model of the circular array's sensor dislocation and the statistical model of the measured data. Section III presents the newly derived hybrid Cramér-Rao bounds (HCRBs) and analyzes its qualitative characteristics. (The detailed derivation of the HCRBs may be found in the Appendix.) Section IV discusses the special case where every sensor's dislocation statistics is the *same* along any of the three Cartesian coordinates. Section V discusses the special case where the dislocation is limited to the circle's Cartesian plane (i.e., with no vertical component), and compares this 2D dislocation case to the *three*-dimensional (3D) case of Sec. IV. Section VI verifies these newly derived Cramér-Rao bounds by showing Monte Carlo simulations of the maximum *a posteriori* (MAP) estimation asymptotically approaching the bounds. Section VII concludes this investigation.

II. THE MEASUREMENT DATA MODEL

Suppose L isotropic sensors are positioned nominally on a circle of radius R with equal inter-sensor spacing. The ℓth sensor's nominal position may be represented as $(R\cos(2\pi(\ell-1)/L), R\sin(2\pi(\ell-1)/L), 0)$ in the 3D Cartesian coordinates, for $\ell \in \{0, 1, \ldots, L-1\}$. Please see Fig. 1(a).

Real-world manufacturing and field deployment, however, are imperfect; the sensors may deviate from their nominal positions mentioned above. Model the ℓth sensor's dislocation as random in *3*D space with the deviation along the x-, y-, and z-axes mathematically represented by the respective stochastic scalars of Δ_{x_ℓ}, Δ_{y_ℓ}, and Δ_{z_ℓ}. This down-to-earth 3D dislocation modeling has never been studied (whether analytically or via simulations) in the entire open literature of UCA direction-finding Cramér-Rao bound analysis to the best of the present authors' knowledge.

Upon this L-element circular array of isotropic sensors, suppose that a point-size emitter impinges from the far field at a wavelength of λ, an azimuth angle of $\phi \in [0, 2\pi)$, and a polar angle (also known as zenith angle) of $\theta \in [0, \pi]$. Then, the $L \times 1$ array manifold would have an ℓth entry of $[\mathbf{a}]_\ell = e^{j\gamma_\ell}$, where

$$\gamma_\ell = \frac{2\pi}{\lambda}\left[R\,\sin(\theta)\cos\left(\phi - \frac{2\pi(\ell-1)}{L}\right) + \sin(\theta)\cos(\phi)\Delta_{x_\ell} + \sin(\theta)\sin(\phi)\Delta_{y_\ell} + \cos(\theta)\Delta_{z_\ell}\right] \quad (1)$$

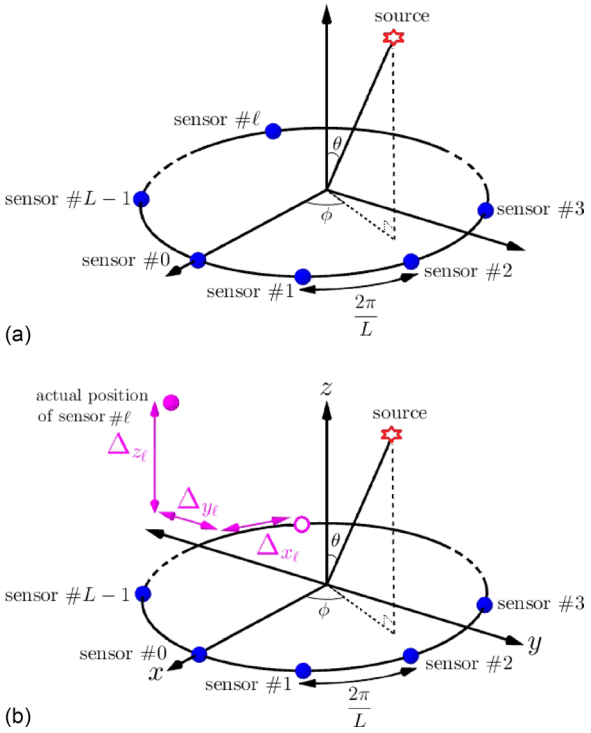

FIG. 1. (Color online) A circular array consisting of L sensors, uniformly spaced on the circumference. (a) All L number of sensors lie precisely at their nominal positions. (b) Sensor ℓ suffers 3D dislocation, from its nominal position (indicated by the open purple circle) to an actual position indicated by the solid purple circle.

for all $\ell \in \{1, 2, \ldots, L\}$. Please see Fig. 1(b). Each sensor's dislocation is thus allowed to be 3D, as opposed to the 2D restriction in Refs. 30, 31, and 33 (which plot the CRB, but present no CRB derivation and no CRB expression).

These $3L$ random variables in $\{\Delta_{x_\ell}, \Delta_{y_\ell}, \Delta_{z_\ell}, \forall \ell = 1, 2, \ldots, L\}$ are modeled stochastically as independent identically distributed Gaussian random scalars with a mean of zero. Moreover, let Δ_{x_ℓ} (Δ_{y_ℓ}, Δ_{z_ℓ}) have a variance of σ_x^2 (σ_y^2, σ_z^2), $\forall \ell$. The statistical model of sensor dislocation in the abovementioned[30,31,33] could be construed as a special case of the general model in this present paper by setting $\sigma_z = 0$.

At the mth time instant, the overall circular array collects this $L \times 1$ vector of data

$$\mathbf{z}(m) = \mathbf{a}s(m) + \mathbf{n}(m) \quad \text{for} \quad m = 1, 2, \ldots, M. \quad (2)$$

To facilitate subsequent analysis on the entire M-sample dataset, define

$$\tilde{\mathbf{z}} := \left[\mathbf{z}^T(1), \mathbf{z}^T(2), \ldots, \mathbf{z}^T(M)\right]^T,$$

$$\mathbf{s} := [s(1), s(2), \ldots, s(M)]^T,$$

$$\tilde{\mathbf{n}} := \left[\mathbf{n}^T(1), \mathbf{n}^T(2), \ldots, \mathbf{n}^T(M)\right]^T.$$

Hence, Eq. (2) may be rewritten as

$$\tilde{\mathbf{z}} = \mathbf{s} \otimes \mathbf{a} + \tilde{\mathbf{n}},$$

where $\otimes$ refers to the Kronecker product.

"Direction finding" aims to estimate an incident source's azimuth-polar direction-of-arrival (ϕ,θ) from the data $\tilde{\mathbf{z}}$, here, despite the sensors' unknown and stochastic dislocations of $\{(\Delta_{x_\ell},\Delta_{y_\ell},\Delta_{z_\ell}),\forall\ell\}$.

To avoid unnecessary distraction from the present focus on the effects of sensor dislocation, a simple signal/noise statistical model will be used:

(i) The incident signal is a complex-valued sinusoid $s(m)=\sigma_s e^{j(2\pi fm+\varphi)}$, where the amplitude σ_s, frequency f, and phase φ are prior known;

(ii) The additive noise $\mathbf{n}(m)$ is modeled as complex-valued, Gaussian, zero in mean, with a prior known variance of σ_n^2, and statistically uncorrelated over time (i.e., over m) and space (i.e., over ℓ).

III. THE NEWLY DERIVED HCRBs

The Appendix has analytically derived the HCRBs in closed forms explicitly in terms of the model parameters

$$\mathrm{HCRB}(\theta)=\frac{1}{L}\frac{1}{\mathrm{SNR}_{\mathrm{eff}}}\frac{1}{2g\left(\theta\pm\frac{\pi}{2},\phi\right)+\frac{(R/\lambda)^2\cos^2(\theta)}{1+2\mathrm{SNR}_{\mathrm{eff}}g(\theta,\phi)}}=\frac{1}{L}\frac{1}{\mathrm{SNR}_{\mathrm{eff}}}\frac{1}{2a_{\parallel}+\frac{\left(\frac{R}{\lambda}\cos(\theta)\right)^2}{1+2\mathrm{SNR}_{\mathrm{eff}}a_{\perp}}},\tag{3}$$

$$\mathrm{HCRB}(\phi)=\frac{1}{L}\frac{\csc^2(\theta)}{\mathrm{SNR}_{\mathrm{eff}}}\frac{1}{2g\left(\pm\frac{\pi}{2},\phi\pm\frac{\pi}{2}\right)+\frac{(R/\lambda)^2}{1+2\mathrm{SNR}_{\mathrm{eff}}g(\theta,\phi)}}=\frac{1}{L}\frac{1}{\mathrm{SNR}_{\mathrm{eff}}}\frac{1}{2a_{x,y}+\frac{\left(\frac{R}{\lambda}\sin(\theta)\right)^2}{1+2\mathrm{SNR}_{\mathrm{eff}}a_{\perp}}},\tag{4}$$

where

$$\mathrm{SNR}_{\mathrm{eff}}:=M\left(2\pi\frac{\sigma_s}{\sigma_n}\right)^2,$$

$$a_{\perp}:=g(\theta,\phi),$$

$$a_{\parallel}:=\cos^2(\theta)\left[\left(\frac{\sigma_{\Delta x}}{\lambda}\cos(\phi)\right)^2+\left(\frac{\sigma_{\Delta y}}{\lambda}\sin(\phi)\right)^2\right]+\left(\frac{\sigma_{\Delta z}}{\lambda}\sin(\theta)\right)^2=g\left(\theta\pm\frac{\pi}{2},\phi\right),$$

$$a_{x,y}:=\left(\frac{\sigma_{\Delta x}}{\lambda}\sin(\phi)\right)^2+\left(\frac{\sigma_{\Delta y}}{\lambda}\cos(\phi)\right)^2=g\left(\pm\frac{\pi}{2},\phi\pm\frac{\pi}{2}\right),$$

$$g(\theta,\phi):=\sin^2(\theta)\left[\left(\frac{\sigma_{\Delta x}}{\lambda}\cos(\phi)\right)^2+\left(\frac{\sigma_{\Delta y}}{\lambda}\sin(\phi)\right)^2\right]+\left(\frac{\sigma_{\Delta z}}{\lambda}\cos(\theta)\right)^2\geq 0,\quad\forall(\theta,\phi).$$

HCRB(θ) of Eq. (3) and HCRB(ϕ) of Eq. (4) share a similar mathematical form: These two expressions would be identical, with the former's a_z and $(R/\lambda)\cos(\theta)$ becoming, respectively, the latter's $a_{x,y}$ and $(R/\lambda)\sin(\theta)$. These two HCRB expressions in Eqs. (3) and (4) both have 8 degrees of freedom: L, $\mathrm{SNR}_{\mathrm{eff}}$, R/λ, $\sigma_{\Delta x}/\lambda$, $\sigma_{\Delta y}/\lambda$, $\sigma_{\Delta z}/\lambda$, θ, and ϕ.

Figure 2 plots HCRB(θ) of Eq. (3) and HCRB(ϕ) of Eq. (4) versus $\sigma_{\Delta x}/\lambda=\sigma_{\Delta y}/\lambda$, and versus $\sigma_{\Delta z}/\lambda$. The following may be observed.

LHCRB(θ) increases with an increasing $\sigma_{\Delta x}/\lambda=\sigma_{\Delta y}/\lambda$ or $\sigma_{\Delta z}/\lambda$, up to local maxima and decreases thereafter. Observe that an increase in $\sigma_{\Delta x}/\lambda=\sigma_{\Delta y}/\lambda$ or $\sigma_{\Delta z}/\lambda$ has a double effect: array geometry perturbation and aperture enlargement. The array geometry perturbation is more pronounced at small values of $\sigma_{\Delta x}/\lambda=\sigma_{\Delta y}/\lambda$ or $\sigma_{\Delta z}/\lambda$, thereby increasing LHCRB(θ). Similarly, at large values of $\sigma_{\Delta x}/\lambda=\sigma_{\Delta y}/\lambda$ or $\sigma_{\Delta z}/\lambda$, the array aperture increment dominates, hence, decreasing LHCRB(θ).

The above explanation also holds for LHCRB(ϕ) nonmonotonic change induced by a varying $\sigma_{\Delta x}/\lambda=\sigma_{\Delta y}/\lambda$. However, LHCRB(ϕ) monotonically increases with an increasing $\sigma_{\Delta z}/\lambda$. This observation is not surprising, recall that the effective aperture for azimuth estimation lies on the x–y plane, hence, an increase in $\sigma_{\Delta x}/\lambda$ or $\sigma_{\Delta y}/\lambda$ would increase/decrease the effective aperture, whereas an increasing $\sigma_{\Delta z}/\lambda$ offers no increment in effective aperture but rather increases the array perturbations.

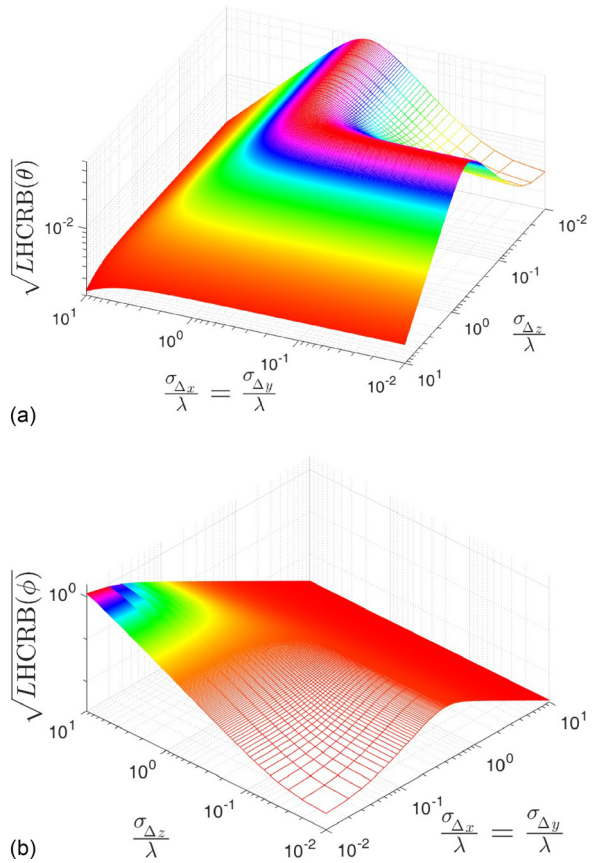

FIG. 2. (Color online) How HCRB(θ) of Eq. (3) and HCRB(ϕ) of Eq. (4) vary with $\sigma_{\Delta x}/\lambda=\sigma_{\Delta y}/\lambda$ and $\sigma_{\Delta z}/\lambda$ at $\mathrm{SNR}_{\mathrm{eff}}=1000$, $\theta=45°$, and $\phi=60°$.

The following qualitative trends may be observed:

(i) *The effects of the sensors' dislocation projected onto the wavefront*—HCRB(θ) decreases (i.e., improves) with an increasing $a_{\|}$, which corresponds to the sensors' dislocation projected onto the incident wavefront (i.e., perpendicular to the incident direction). Such projected dislocations would enlarge (over the sensors' random dislocation's "probability space" as a whole) the array's effective aperture with respect to the wavefront. Hence, HCRB(θ) improves as $a_{\|}$ increases.

(ii) *The effects of the sensors' dislocation projected onto the incident signal's propagation direction*—Both HCRB(θ) and HCRB(ϕ) increase (i.e., worsen) with a *larger* $a_{\perp}$, which corresponds to the sensors' dislocation projected *perpendicular* to the incident wavefront (i.e., onto the incident wavefront's incident direction). Therefore, $a_{\perp}$ would *not* enlarge/contract the array's effective aperture *along* the wavefront. Instead, $a_{\perp}$ represents the sensor dislocation's nuisance effects in the hybrid Fisher information. Hence, HCRB(θ) increases (i.e., worsens) as $a_{\perp}$ increases.

(iii) *The effects of the sensors' dislocation projected onto the circle's horizontal aperture*—Counterpart to point (i) above: HCRB(ϕ) decreases (i.e., improves) with a larger $a_{x,y}$, which corresponds to the sensors' dislocation projected onto the circular array aperture (i.e., the x–y plane).

(iv) *The effects of the sensors' dislocation projected vertically in perpendicular to the circle's aperture*—The σ_z term (which is present in $a_{\|}$ and $a_{\perp}$) is absent in $a_{x,y}$. Hence, the sensors' vertical dislocation along the z axis (i.e., in perpendicular to the circular array's aperture) cannot improve HCRB(ϕ) through $a_{x,y}$, but can only degrade HCRB(ϕ) through $a_{\perp}$ due to the nuisance-parameter effect mentioned in point (ii) above.

(v) *The effects of* $\mathrm{SNR}_{\mathrm{eff}}$—Both HCRB($\theta$) and HCRB($\phi$) expectedly decrease (i.e., improve) with an increasing $\mathrm{SNR}_{\mathrm{eff}}$, with all other parameters remaining the same. Furthermore, $\mathrm{SNR}_{\mathrm{eff}}$ amplifies the positive effects of the sensors' dislocation discussed above under points (i) and (iii), but diminishes the negative effects of the sensors' dislocation discussed above under point (ii).

(vi) Both HCRB(θ) and HCRB(ϕ) decrease (i.e., improve) with a larger $\pi(R/\lambda)^2$, which is the circular array's wavelength-normalized aperture area. However, the array's physical aperture affects the two HCRBs somewhat differently:

(vi-a) The circular aperture (of wavelength-normalized radius R/λ) raises HCRB(θ) only through $(R/\lambda)\cos(\theta)$, which represents the projection of the array's physical aperture onto the z axis, against which the polar direction-of-arrival (θ) has been defined.

(vi-b) The circular aperture raises HCRB(ϕ) only through $(R/\lambda)\sin(\theta)$, which constitutes the projection of the array's physical aperture onto the x–y plane, on which the azimuthal direction-of-arrival (ϕ) is measured.

The incident source's direction-of-arrival affects the HCRBs also through points (i) and (ii) above.

(vii) Both HCRB(θ) and HCRB(ϕ) are inversely proportional to the number (L) of sensors comprising the circular array, with all other parameters kept constant. This trend is anticipated, as a larger aperture facilitates a finer resolution of the arrival direction. Indeed, as $L \to \infty$, HCRB(θ) and HCRB(ϕ) both converge to zero.

IV. HCRB FOR SENSOR DISLOCATION WHOSE STATISTICAL VARIANCE IS SPATIALLY ISOTROPIC

Here, $\sigma_x^2 = \sigma_{\Delta y}^2 = \sigma_{\Delta z}^2 = \sigma_{\Delta}^2$. Then, Eqs. (3) and (4) simplify to

$$\mathrm{HCRB}_{\mathrm{same}}(\theta) = \frac{1}{L}\frac{1}{\mathrm{SNR}_{\mathrm{eff}}}\left[2\left(\frac{\sigma_{\Delta}}{\lambda}\right)^2 + \frac{\left(\frac{R}{\lambda}\right)^2\cos^2(\theta)}{2\mathrm{SNR}_{\mathrm{eff}}\left(\frac{\sigma_{\Delta}}{\lambda}\right)^2 + 1}\right]^{-1} = \frac{1}{L}\left[\tilde{\sigma}_{\Delta} + \frac{\tilde{R}\cos^2(\theta)}{1+\tilde{\sigma}_{\Delta}}\right]^{-1}, \tag{5}$$

$$\mathrm{HCRB}_{\mathrm{same}}(\phi) = \frac{1}{L\mathrm{SNR}_{\mathrm{eff}}}\frac{\csc^2(\theta)}{2\left(\frac{\sigma_{\Delta}}{\lambda}\right)^2 + \frac{\left(\frac{R}{\lambda}\right)^2}{2\mathrm{SNR}_{\mathrm{eff}}\left(\frac{\sigma_{\Delta}}{\lambda}\right)^2 + 1}} = \frac{\sec^2(\theta)}{L}\left[\tilde{\sigma}_{\Delta} + \frac{\tilde{R}}{1+\tilde{\sigma}_{\Delta}}\right]^{-1}, \tag{6}$$

where

$$\tilde{R} := \mathrm{SNR}_{\mathrm{eff}}\left(\frac{R}{\lambda}\right)^2, \tag{7}$$

$$\tilde{\sigma}_{\Delta} := 2\mathrm{SNR}_{\mathrm{eff}}\left(\frac{\sigma_{\Delta}}{\lambda}\right)^2. \tag{8}$$

As $\sigma_{\Delta x}^2 = \sigma_{\Delta y}^2 = \sigma_{\Delta z}^2 = \sigma_{\Delta}^2$, both $a_{\perp}$ and $a_{\|}$ in Eq. (3) "collapse" into the same entity of $\tilde{\sigma}_{\Delta}$ in Eq. (5), even though $a_{\|}$ and $a_{\perp}$ produce opposing effects on HCRB(θ). [Recall from points (i) and (ii) in Sec. III that HCRB(θ) decreases (i.e., improves) with a larger $a_{\|}$ but with a smaller $a_{\perp}$.] This accounts for the non-monotonic dependence on $\tilde{\sigma}_{\Delta}$ in Fig. 3.

Similarly, both $a_{x,y}$ and $a_{\perp}$ in Eq. (4) here "collapse" into the same entity of $\tilde{\sigma}_{\Delta}$ in Eq. (6), even though $a_{\perp}$ and $a_{\|}$ produce opposing effects on HCRB (ϕ) as discussed in points (ii) and (iii) in Sec. III. Indeed, if $L\cos^2(\theta)\,\mathrm{HCRB}_{\mathrm{same}}(\phi)$ is plotted in a 3D graph against $\tilde{R}$ and $\tilde{\sigma}_{\Delta}$, then that graph would look exactly the same as Fig. 3 with $\tilde{R}$ replacing $\tilde{R}\cos^2(\theta)$.

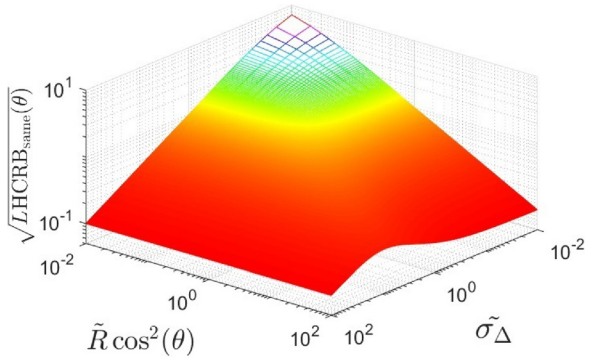

FIG. 3. (Color online) How $\sqrt{L\,\mathrm{HCRB}_{3\mathrm{D}}(\theta)}$ of Eq. (5) varies with its two degrees of freedom.

If all sensors are perfectly positioned at their nominal locations, $\sigma_\Delta^2 = 0$, Eqs. (5) and (6) would then degenerate to

$$\mathrm{HCRB}(\theta) \to \frac{1}{L\mathrm{SNR}_{\mathrm{eff}}}\left(\frac{R}{\lambda}\right)^{-2}\sec^2(\theta), \tag{9}$$

$$\mathrm{HCRB}(\phi) \to \frac{1}{L\mathrm{SNR}_{\mathrm{eff}}}\left(\frac{R}{\lambda}\right)^{-2}\csc^2(\theta). \tag{10}$$

These asymptotic expressions in Eqs. (9) and (10) agree with Eqs. (27) and (28) of Ref. 15 and Eq. (1.149) of Ref. 61 (p. 43).[62]

If $\sigma_\Delta^2 \to \infty$, the sensor mislocations become infinite, then $\mathrm{HCRB}(\theta)$ and $\mathrm{HCRB}(\phi)$ both would become zero. This surprising trend is due to the theoretically infinite aperture thus realized.

V. HCRBS IF $\sigma_{\Delta_x}=\sigma_{\Delta_y}=\sigma_\Delta$ BUT $\sigma_{\Delta_z}=0$

If $\sigma_{\Delta_x}^2 = \sigma_{\Delta_y}^2 = \sigma_\Delta^2$ but $\sigma_{\Delta_z}^2 = 0$, the sensors' dislocation would be limited to only the circle's Cartesian plane and would have no vertical component.[63] Then, Eqs. (3) and (4) simplify to Eqs. (11) and (12), respectively,

$$L\mathrm{HCRB}_{2\mathrm{D}}(\theta) = \frac{\mathrm{SNR}_{\mathrm{eff}}^{-1}}{2\left(\frac{\sigma_\Delta}{\lambda}\right)^2\cos^2(\theta) + \frac{(R/\lambda)^2\cos^2(\theta)}{1+2\mathrm{SNR}_{\mathrm{eff}}\left(\frac{\sigma_\Delta}{\lambda}\right)^2\sin^2(\theta)}}$$

$$= \frac{\sec^2(\theta)}{\tilde{\sigma}_\Delta + \frac{\tilde{R}}{1+\tilde{\sigma}_\Delta\sin^2(\theta)}}, \tag{11}$$

$$L\mathrm{HCRB}_{2\mathrm{D}}(\phi) = \frac{\mathrm{SNR}_{\mathrm{eff}}^{-1}\csc^2(\theta)}{2\left(\frac{\sigma_\Delta}{\lambda}\right)^2 + \frac{(R/\lambda)^2}{1+2\mathrm{SNR}_{\mathrm{eff}}\left(\frac{\sigma_\Delta}{\lambda}\right)^2\sin^2(\theta)}}$$

$$= \frac{\csc^2(\theta)}{\tilde{\sigma}_\Delta + \frac{\tilde{R}}{1+\tilde{\sigma}_\Delta\sin^2\theta}}. \tag{12}$$

The denominators are the same in Eqs. (11) and (12).

Perhaps surprising to some readers, 3D sensor dislocation could *improve* the HRCB of θ over 2D dislocation. That is, $\mathrm{HCRB}_{\mathrm{same}}(\theta) < \mathrm{HCRB}_{2\mathrm{D}}(\theta)$, for some $\tilde{\sigma}_\Delta > 0$. The proof follows:

$$\mathrm{HCRB}_{\mathrm{same}}(\theta) - \mathrm{HCRB}_{2\mathrm{D}}(\theta) = \frac{1}{L}\frac{\tilde{R}\cos^4(\theta) - \sin^2(\theta)(1+\tilde{\sigma}_\Delta)\left(1+\sin^2(\theta)\tilde{\sigma}_\Delta\right)}{\frac{\cos^2(\theta)}{\tilde{\sigma}_\Delta}\left(\tilde{\sigma}_\Delta + \tilde{\sigma}_\Delta^2\sin^2(\theta) + \tilde{R}\right)\left(\tilde{\sigma}_\Delta + \tilde{\sigma}_\Delta^2 + \tilde{R}\,\cos^2(\theta)\right)}. \tag{13}$$

The denominator in Eq. (13) is obviously positive for all $\theta, \tilde{\sigma}_\Delta, \tilde{R}$. Define the numerator as $g_\theta(\tilde{\sigma}_\Delta)$. Observe that

$$\frac{d}{d\tilde{\sigma}_\Delta}g_\theta(\tilde{\sigma}_\Delta) = -\sin^2(\theta)\left(1+\sin^2(\theta)+2\sin^2(\theta)\tilde{\sigma}_\Delta\right) < 0, \quad \forall\tilde{\sigma}_\Delta.$$

Hence, $g_\theta(\tilde{\sigma}_\Delta)$ is monotonically decreasing in $\tilde{\sigma}_\Delta$. Furthermore, $g_\theta(\tilde{\sigma}_\Delta) = 0$ has non-negative real-valued roots at $\tilde{\sigma}_\Delta = 0$ and

$$\tilde{\sigma}_\Delta = \frac{\sin(2\theta)\sqrt{\cos^2(\theta)(1+4\tilde{R}) - 1 - \sin^2(\theta)}}{4\sin^3(\theta)}.$$

Therefore, $\mathrm{HCRB}_{2\mathrm{D}}(\theta) > \mathrm{HCRB}_{\mathrm{same}}(\theta)$ for all $\theta, \tilde{R}$ and only for all

$$\tilde{\sigma}_\Delta > \frac{\sin(2\theta)\sqrt{\cos^2(\theta)(1+4\tilde{R}) - 1 - \sin^2(\theta)}}{4\sin^3(\theta)}.$$

Furthermore, $\mathrm{HCRB}_{2\mathrm{D}}(\theta) = \mathrm{HCRB}_{\mathrm{same}}(\theta)$ if $\tilde{\sigma}_\Delta$ equals the threshold.

As for the HRCB of ϕ, 3D sensor dislocation is always worse than the 2D case. That is, $\mathrm{HCRB}_{\mathrm{same}}(\phi) \geq \mathrm{HCRB}_{2\mathrm{D}}(\phi), \forall\tilde{\sigma}_\Delta > 0$. The proof follows:

$$\mathrm{HCRB}_{\mathrm{same}}(\phi) - \mathrm{HCRB}_{\mathrm{2D}}(\phi) = \frac{1}{L}\frac{\tilde{R}\cot^2(\theta)\tilde{\sigma}_\Delta}{\left(\tilde{\sigma}_\Delta + \tilde{\sigma}_\Delta^2 + \tilde{R}\right)\left(\tilde{\sigma}_\Delta + \sin^2(\theta)\tilde{\sigma}_\Delta + \tilde{R}\right)}, \tag{14}$$

which is positive for all $\tilde{\sigma}_\Delta > 0, \tilde{R}, \theta$. Furthermore,

$$\lim_{\tilde{\sigma}_\Delta \to \infty}\left[\mathrm{HCRB}_{\mathrm{same}}(\phi) - \mathrm{HCRB}_{\mathrm{2D}}(\phi)\right] = 0$$
$$\Rightarrow \mathrm{HCRB}_{\mathrm{same}}(\phi) \to \mathrm{HCRB}_{\mathrm{2D}}(\phi) \quad \text{as} \quad \tilde{\sigma}_\Delta \to \infty.$$

VI. MAP ESTIMATION VERIFIES THE DERIVED HCRBs

The HCRB is approached by MAP estimation, asymptotically as the effective signal-to-noise power ratio $[\mathrm{SNR}_{\mathrm{eff}} := M(2\pi\sigma_s/\sigma_n)^2]$ approaches infinity and as sensor dislocation σ_Δ/λ approaches zero. (Please see Sec. IV, p. 2079 of Ref. 64.) Monte Carlo simulations in this section will indeed show this agreement with the HCRB expressions derived in Eqs. (3) and (4), thereby verifying the correctness of the derivation.

The MAP estimate maximizes the posterior probability density function of $[\theta, \phi, \mathbf{\Delta}]$, given the observation $\tilde{\mathbf{z}}$. $\mathbf{\Delta}$ is defined in the Appendix. The following develops the MAP estimator given the statistical model of the sensor dislocation, the signal, and the noise of Sec. II. This data's posterior probability function equals

$$p(\theta, \phi, \mathbf{\Delta}|\tilde{\mathbf{z}}) \propto p(\tilde{\mathbf{z}}, \theta, \phi, \mathbf{\Delta}) = p(\tilde{\mathbf{z}}|\theta, \phi, \mathbf{\Delta})p(\mathbf{\Delta}),$$

where

$$p(\tilde{\mathbf{z}}|\theta, \phi, \mathbf{\Delta}) = \frac{1}{|\pi\Gamma|}\exp\left\{-[\tilde{\mathbf{z}} - \mathbf{s}\otimes\mathbf{a}]^H\Gamma^{-1}[\tilde{\mathbf{z}} - \mathbf{s}\otimes\mathbf{a}]\right\}$$

refers to the conditional probability density of $\tilde{\mathbf{z}}$ conditioned on $(\theta, \phi, \mathbf{\Delta})$, and

$$\begin{aligned} p(\mathbf{\Delta}) &= \left(\prod_{\ell=1}^{L}\frac{1}{\sqrt{2\pi\sigma_{\Delta x}^2}}e^{-\Delta_{x_\ell}^2/2\sigma_{\Delta x}^2}\right) \\ &\quad\times\left(\prod_{\ell=1}^{L}\frac{1}{\sqrt{2\pi\sigma_{\Delta y}^2}}e^{-\Delta_{y_\ell}^2/2\sigma_{\Delta y}^2}\right) \\ &\quad\times\left(\prod_{\ell=1}^{L}\frac{1}{\sqrt{2\pi\sigma_{\Delta z}^2}}e^{-\Delta_{z_\ell}^2/2\sigma_{\Delta z}^2}\right) \\ &= \left(2\pi\sigma_{\Delta x}^2\right)^{-L/2}\left(2\pi\sigma_{\Delta y}^2\right)^{-L/2}\left(2\pi\sigma_{\Delta z}^2\right)^{-L/2} \\ &\quad\times\exp\left\{-\frac{1}{2}\sum_{\ell=1}^{L}\left(\frac{\Delta_{x_\ell}^2}{\sigma_{\Delta x}^2} + \frac{\Delta_{y_\ell}^2}{\sigma_{\Delta y}^2} + \frac{\Delta_{z_\ell}^2}{\sigma_{\Delta z}^2}\right)\right\} \end{aligned}$$

denotes the prior probability density function of $\mathbf{\Delta}$. Hence,

$$\begin{aligned} p(\theta, \phi, \mathbf{\Delta}|\tilde{\mathbf{z}}) &\propto p(\tilde{\mathbf{z}}, \theta, \phi, \mathbf{\Delta}) \\ &= p(\tilde{\mathbf{z}}|\theta, \phi, \mathbf{\Delta})p(\mathbf{\Delta}) \\ &= \frac{1}{|\pi\Gamma|}\exp\left\{-[\tilde{\mathbf{z}} - \mathbf{s}\otimes\mathbf{a}]^H\Gamma^{-1}[\tilde{\mathbf{z}} - \mathbf{s}\otimes\mathbf{a}]\right\} \\ &\quad\times\left(2\pi\right)^{-3L/2}\left(\sigma_{\Delta x}\sigma_{\Delta y}\sigma_{\Delta z}\right)^{-L} \\ &\quad\times\exp\left\{-\frac{1}{2}\sum_{\ell=1}^{L}\left(\frac{\Delta_{x_\ell}^2}{\sigma_{\Delta x}^2} + \frac{\Delta_{y_\ell}^2}{\sigma_{\Delta y}^2} + \frac{\Delta_{z_\ell}^2}{\sigma_{\Delta z}^2}\right)\right\} \\ &= \frac{1}{|\pi\Gamma|}\left(2\pi\right)^{-3L/2}\left(\sigma_{\Delta x}\sigma_{\Delta y}\sigma_{\Delta z}\right)^{-L} \\ &\quad\times\exp\left\{-\left[\frac{1}{\sigma_n^2}[\tilde{\mathbf{z}} - \mathbf{s}\otimes\mathbf{a}]^H[\tilde{\mathbf{z}} - \mathbf{s}\otimes\mathbf{a}]\right.\right. \\ &\quad\left.\left.+\frac{1}{2}\sum_{\ell=1}^{L}\left(\frac{\Delta_{x_\ell}^2}{\sigma_{\Delta x}^2} + \frac{\Delta_{y_\ell}^2}{\sigma_{\Delta y}^2} + \frac{\Delta_{z_\ell}^2}{\sigma_{\Delta z}^2}\right)\right]\right\}. \end{aligned}$$

Therefore, the MAP estimate equals

$$\begin{aligned} \left(\hat{\theta}, \hat{\phi}, \hat{\mathbf{\Delta}}\right) &= \arg\max_{(\theta,\phi,\Delta)} p(\theta, \phi, \mathbf{\Delta}|\tilde{\mathbf{z}}) \\ &= \arg\max_{(\theta,\phi,\Delta)} p(\tilde{\mathbf{z}}|\theta, \phi, \mathbf{\Delta})p(\mathbf{\Delta}) \\ &= \arg\min_{(\theta,\phi,\mathbf{\Delta})}\left\{\frac{1}{\sigma_n^2}[\tilde{\mathbf{z}} - \mathbf{s}\otimes\mathbf{a}]^H[\tilde{\mathbf{z}} - \mathbf{s}\otimes\mathbf{a}]\right. \\ &\quad\left.+\frac{1}{2}\sum_{\ell=1}^{L}\left(\frac{\Delta_{x_\ell}^2}{\sigma_{\Delta x}^2} + \frac{\Delta_{y_\ell}^2}{\sigma_{\Delta y}^2} + \frac{\Delta_{z_\ell}^2}{\sigma_{\Delta z}^2}\right)\right\}. \end{aligned} \tag{15}$$

This MAP estimation is Monte Carlo simulated, with the resulting root-mean-square error (RMSE) plotted in Figs. 4 and 5. Here, each icon represents $N = 3000$ statistically independent Monte Carlo experiments, each involving $M = 100$ snapshots. The circular array consists of $L = 40$ identical isotropic sensors, nominally spaced uniformly at half-wavelength inter-sensor spacing on a circle of wavelength-radius $R/\lambda = \frac{1}{4}\csc(\pi/L)$. The incident signal has a frequency of $f = 0.25$, a wavelength of $\lambda = 0.0344$, an initial phase of $\psi = 0.23\pi$, a power of $\sigma_s^2 = 1$, an incident

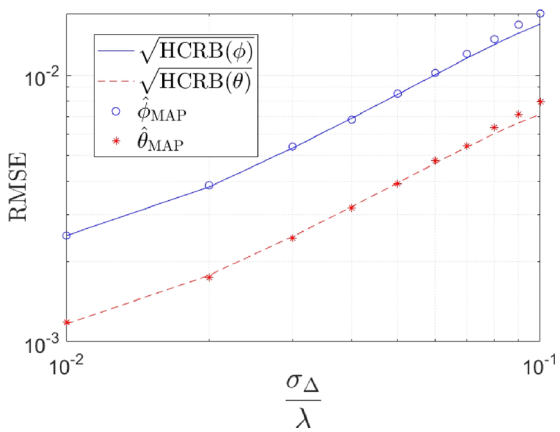

FIG. 4. (Color online) The MAP estimates approach the HCRB(θ) of Eq. (5) and the HCRB(ϕ) of Eq. (6) as the sensor dislocation variance $(\sigma_\Delta/\lambda)^2 \to 0$. There exist $M = 100$ snapshots in each Monte Carlo trial.

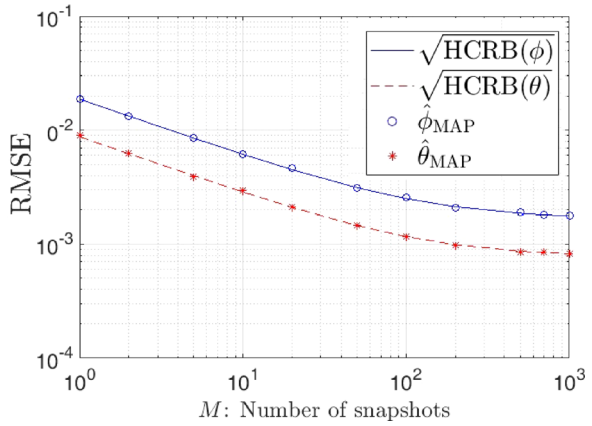

FIG. 5. (Color online) The MAP estimates approach the HCRB(θ) of Eq. (5) and the HCRB(ϕ) of Eq. (6), as the number M of snapshots increases. Here, $\sigma_\Delta/\lambda = 1/100$.

polar angle of $\theta = 25°$, and an incident azimuth angle of $\phi = 43°$. The additive noise has a power of $\sigma_n^2 = 1$. The RMSE is defined as $\sqrt{(1/N)\sum_{n=1}^{N}(\hat{\theta}_n - \theta)^2}$ for $\hat{\theta}$, and $\sqrt{(1/N)\sum_{n=1}^{N}(\hat{\phi}_n - \phi)^2}$ for $\hat{\phi}$. Figures 4 and 5 clearly show that the MAP estimates approach the derived HCRBs especially at the asymptotically small σ_Δ/λ or with asymptotically large number (M) of snapshots.

VII. CONCLUSIONS

This paper presents the open literature's first rigorous derivation of any HCRB for azimuth-elevation direction-of-arrival estimation with a circular array of identical isotropic sensors that are nominally uniform in spacing but actually dislocate randomly. This derivation leads to some surprising qualitative insights: (a) The incident source's polar-arrival-angle HCRB is *enhanced* as the sensors become *more* dislocated *along the wavefront* due to aperture enlargement over the stochastic dislocation's probability space. (b) Likewise, the azimuth-arrival-angle's HCRB is *improved* as the sensors become *more* dislocated *on the circular array's plane*, also due to aperture enlargement. (c) In contrast, sensor dislocation *along the incident signal's propagation direction* can only worsen the HCRBs, due to nuisance-parameter effects in the Fisher information. (d) However, sensor dislocation *orthogonal to the circular array's plane* must degrade the azimuth-arrival-angle HCRB but could improve the polar-arrival-angle HCRB.

APPENDIX: DETAILED DERIVATION OF THE HCRBs

1. To formulate the hybrid Fisher information matrix

Group all $2+3L$ unknown scalars into a $(2+3L)\times 1$ vector of $\boldsymbol{\xi} := [\theta, \phi, \boldsymbol{\Delta}]^T$, in which $\boldsymbol{\Delta} := [\Delta_{x_1}, \Delta_{x_2}, \ldots, \Delta_{x_L}, \Delta_{y_1}, \ldots, \Delta_{y_L}, \Delta_{z_1}, \ldots, \Delta_{z_L}]$ contains all the nuisance parameters, which also happen to be stochastic.

The probability density function of $\tilde{\mathbf{z}}$, conditioned on $\boldsymbol{\Delta}$, equals

$$p(\tilde{\mathbf{z}}|\boldsymbol{\Delta}) = \frac{1}{|\pi\Gamma|}\exp\left\{-[\tilde{\mathbf{z}} - \boldsymbol{\mu}]^H \Gamma^{-1}[\tilde{\mathbf{z}} - \boldsymbol{\mu}]\right\},$$

which has a statistical conditional mean equal to the $LM \times 1$ vector of

$$\begin{aligned}\boldsymbol{\mu} &= E_{\tilde{\mathbf{z}}|\Delta}[\tilde{\mathbf{z}}|\boldsymbol{\Delta}] \\ &= \mathbf{s} \otimes \mathbf{a} + E[\tilde{\mathbf{n}}] \\ &= \mathbf{s} \otimes \mathbf{a},\end{aligned}$$

and a statistical conditional covariance matrix equal to the $LM \times LM$ matrix of

$$\begin{aligned}\Gamma &= \text{cov}(\tilde{\mathbf{z}}|\boldsymbol{\Delta}) \\ &= E_{\tilde{\mathbf{z}}|\Delta}\{[\tilde{\mathbf{z}} - \boldsymbol{\mu}][\tilde{\mathbf{z}} - \boldsymbol{\mu}]^H\} \\ &= E[\tilde{\mathbf{n}}\tilde{\mathbf{n}}^H] \\ &= \sigma_n^2 \mathbf{I}_{LM\times LM},\end{aligned}$$

where $\mathbf{I}$ symbolizes an identity matrix of the size indicated in its subscript.

For the above conditional probability density, the hybrid Fisher information matrix equals (please see Eqs. 8.49–8.57 in Ref. 65)

$$\mathbf{J}_B = \mathbf{J}_P + \mathbf{J}_D, \tag{A1}$$

where $\mathbf{J}_P$ is a $(3L+2)\times(3L+2)$ matrix corresponding to the *a priori* knowledge on the sensors' dislocation statistics, whereas $\mathbf{J}_D$ is a $(3L+2)\times(3L+2)$ matrix corresponding to the *a posteriori* information embedded in the measured data. The (i,j)th entry equals

$$[\mathbf{J}_P]_{i,j} = -E_\Delta\left[\frac{\partial^2 \ln p_\Delta(\boldsymbol{\Delta})}{\partial\xi_i \partial\xi_j}\right], \tag{A2}$$

$$\begin{aligned}[\mathbf{J}_D]_{i,j} &= -E_{\tilde{\mathbf{z}},\Delta}\left[\frac{\partial^2 \ln p(\tilde{\mathbf{z}}|\boldsymbol{\Delta})}{\partial\xi_i \partial\xi_j}\right] \\ &= E_\Delta\left\{-E_{\tilde{\mathbf{z}}|\Delta}\left[\frac{\partial^2 \ln p(\tilde{\mathbf{z}}|\boldsymbol{\Delta})}{\partial\xi_i \partial\xi_j}\right]\right\},\end{aligned} \tag{A3}$$

where ξ_i denotes the ith entry of the vector $\boldsymbol{\xi}$, and $p_\Delta(\boldsymbol{\Delta})$ signifies the prior probability density function of $\boldsymbol{\Delta}$.

2. To derive $\mathbf{J}_P$

Recall that $\boldsymbol{\Delta}$ is Gaussian with a zero mean and a covariance matrix of $\Gamma_\Delta = \text{diag}(\sigma_{\Delta x}^2 \mathbf{I}_{L\times L}, \sigma_{\Delta y}^2 \mathbf{I}_{L\times L}, \sigma_{\Delta z}^2 \mathbf{I}_{L\times L})$, where diag(·) symbolizes a diagonal matrix with its diagonal entries listed inside the parentheses.

Hence, Eq. (A2) becomes

$$\mathbf{J}_P = \begin{bmatrix} \mathbf{0}_{2\times 2} & \mathbf{0}_{2\times L} & \mathbf{0}_{2\times L} & \mathbf{0}_{2\times L} \\ \mathbf{0}_{L\times 2} & \frac{1}{\sigma_{\Delta x}^2}\mathbf{I}_{L\times L} & \mathbf{0}_{L\times L} & \mathbf{0}_{L\times L} \\ \mathbf{0}_{L\times 2} & \mathbf{0}_{L\times L} & \frac{1}{\sigma_{\Delta y}^2}\mathbf{I}_{L\times L} & \mathbf{0}_{L\times L} \\ \mathbf{0}_{L\times 2} & \mathbf{0}_{L\times L} & \mathbf{0}_{L\times L} & \frac{1}{\sigma_{\Delta z}^2}\mathbf{I}_{L\times L} \end{bmatrix}. \tag{A4}$$

3. To derive $\mathbf{J}_D$

From Eq. (A3) (see Eqs. 8.23–8.34 in Ref. 65),

$$[\mathbf{J}_D]_{\xi_i,\xi_j} = E_\Delta\left[2\mathrm{Re}\left\{\left(\frac{\partial \boldsymbol{\mu}}{\partial \xi_i}\right)^H \boldsymbol{\Gamma}^{-1}\left(\frac{\partial \boldsymbol{\mu}}{\partial \xi_j}\right)\right\} + \mathrm{Tr}\left\{\boldsymbol{\Gamma}^{-1}\left(\frac{\partial \boldsymbol{\Gamma}}{\partial \xi_i}\right)\boldsymbol{\Gamma}^{-1}\left(\frac{\partial \boldsymbol{\Gamma}}{\partial \xi_j}\right)\right\}\right]. \tag{A5}$$

As $\boldsymbol{\Gamma}$ is independent of $\boldsymbol{\xi}$, the trace term drops out above. Hence,

$$[\mathbf{J}_D]_{\xi_i,\xi_j} = E_\Delta\left[2\mathrm{Re}\left\{\left(\frac{\partial \boldsymbol{\mu}}{\partial \xi_i}\right)^H \boldsymbol{\Gamma}^{-1}\left(\frac{\partial \boldsymbol{\mu}}{\partial \xi_j}\right)\right\}\right] = \frac{2}{\sigma_n^2}E_\Delta\left[\underbrace{\mathrm{Re}\left\{\left(\frac{\partial \boldsymbol{\mu}}{\partial \xi_i}\right)^H \left(\frac{\partial \boldsymbol{\mu}}{\partial \xi_j}\right)\right\}}_{h_{i,j}:=}\right]. \tag{A6}$$

The following will express Eq. (A6) explicitly in terms of the parameters of the models in Sec. II.

a. Deriving the partial derivatives

The partial derivatives in Eq. (A6) are given by

$$\frac{\partial \gamma_\ell}{\partial \theta} = \frac{2\pi}{\lambda}\left[R\,\cos(\theta)\cos\left(\phi - \frac{2\pi(\ell-1)}{L}\right) + \cos(\theta)\cos(\phi)\Delta_{x_\ell} + \cos(\theta)\sin(\phi)\Delta_{y_\ell} - \sin(\theta)\Delta_{z_\ell}\right],$$

$$\frac{\partial \gamma_\ell}{\partial \phi} = \frac{2\pi}{\lambda}\left[-R\,\sin(\theta)\sin\left(\phi - \frac{2\pi(\ell-1)}{L}\right) - \sin(\theta)\sin(\phi)\Delta_{x_\ell} + \sin(\theta)\cos(\phi)\Delta_{y_\ell}\right],$$

$$\frac{\partial \gamma_\ell}{\partial \Delta_{x_\ell}} = \frac{2\pi}{\lambda}\sin(\theta)\cos(\phi),$$

$$\frac{\partial \gamma_\ell}{\partial \Delta_{y_\ell}} = \frac{2\pi}{\lambda}\sin(\theta)\sin(\phi),$$

$$\frac{\partial \gamma_\ell}{\partial \Delta_{z_\ell}} = \frac{2\pi}{\lambda}\cos(\theta),$$

$$\frac{\partial \gamma_\ell}{\partial \Delta_{x_m}} = \frac{\partial \gamma_\ell}{\partial \Delta_{y_m}} = \frac{\partial \gamma_\ell}{\partial \Delta_{z_m}} = 0, \quad \forall\, m \neq \ell,$$

$$\frac{\partial [\mathbf{a}]_\ell}{\partial \theta} = j\left(\frac{\partial \gamma_\ell}{\partial \theta}\right)e^{j\gamma_\ell} = j\frac{2\pi}{\lambda}\left[R\,\cos(\theta)\cos\left(\phi - \frac{2\pi(\ell-1)}{L}\right) + \cos(\theta)\cos(\phi)\Delta_{x_\ell} + \cos(\theta)\sin(\phi)\Delta_{y_\ell} - \sin(\theta)\Delta_{z_\ell}\right]e^{j\gamma_\ell},$$

$$\frac{\partial [\mathbf{a}]_\ell}{\partial \phi} = j\left(\frac{\partial \gamma_\ell}{\partial \phi}\right)e^{j\gamma_\ell} = j\frac{2\pi}{\lambda}\left[-R\,\sin(\theta)\sin\left(\phi - \frac{2\pi(\ell-1)}{L}\right) - \sin(\theta)\sin(\phi)\Delta_{x_\ell} + \sin(\theta)\cos(\phi)\Delta_{y_\ell}\right]e^{j\gamma_\ell},$$

$$\frac{\partial [\mathbf{a}]_\ell}{\partial \Delta_{x_\ell}} = j\left(\frac{\partial \gamma_\ell}{\partial \Delta_{x_\ell}}\right)e^{j\gamma_\ell} = j\frac{2\pi}{\lambda}\sin(\theta)\cos(\phi)e^{j\gamma_\ell},$$

$$\frac{\partial [\mathbf{a}]_\ell}{\partial \Delta_{y_\ell}} = j\left(\frac{\partial \gamma_\ell}{\partial \Delta_{y_\ell}}\right)e^{j\gamma_\ell} = j\frac{2\pi}{\lambda}\sin(\theta)\sin(\phi)e^{j\gamma_\ell},$$

$$\frac{\partial [\mathbf{a}]_\ell}{\partial \Delta_{z_\ell}} = j\left(\frac{\partial \gamma_\ell}{\partial \Delta_{z_\ell}}\right)e^{j\gamma_\ell} = j\frac{2\pi}{\lambda}\cos(\theta)e^{j\gamma_\ell},$$

$$\frac{\partial [\mathbf{a}]_\ell}{\partial \Delta_{x_m}} = \frac{\partial [\mathbf{a}]_\ell}{\partial \Delta_{y_m}} = \frac{\partial [\mathbf{a}]_\ell}{\partial \Delta_{z_m}} = 0, \quad \forall m \neq \ell.$$

Thus,

$$\frac{\partial \boldsymbol{\mu}}{\partial \theta} = \mathbf{s} \otimes \frac{\partial \mathbf{a}}{\partial \theta} = \mathbf{s} \otimes j\frac{2\pi}{\lambda}\begin{bmatrix} \left(R\,\cos(\theta)\cos(\phi) + \cos(\theta)\cos(\phi)\Delta_{x_1} + \cos(\theta)\sin(\phi)\Delta_{y_1} - \sin(\theta)\Delta_{z_1}\right)e^{j\gamma_1} \\ \left(R\,\cos(\theta)\cos\left(\phi - \frac{2\pi}{L}\right) + \cos(\theta)\cos(\phi)\Delta_{x_2} + \cos(\theta)\sin(\phi)\Delta_{y_2} - \sin(\theta)\Delta_{z_2}\right)e^{j\gamma_2} \\ \vdots \\ \left(\cos(\theta)\left(R\,\cos\left(\phi - \frac{2\pi(L-1)}{L}\right) + \cos(\phi)\Delta_{x_L} + \sin(\phi)\Delta_{y_L}\right) - \sin(\theta)\Delta_{z_L}\right)e^{j\gamma_L} \end{bmatrix},$$

$$\frac{\partial \boldsymbol{\mu}}{\partial \phi} = \mathbf{s} \otimes \frac{\partial \mathbf{a}}{\partial \phi} = \mathbf{s} \otimes j\frac{2\pi}{\lambda}\begin{bmatrix} \left(-R\,\sin(\theta)\sin(\phi) - \sin(\theta)\sin(\phi)\Delta_{x_1} + \sin(\theta)\cos(\phi)\Delta_{y_1}\right)e^{j\gamma_1} \\ \left(-R\,\sin(\theta)\sin\left(\phi - \frac{2\pi}{L}\right) - \sin(\theta)\sin(\phi)\Delta_{x_2} + \sin(\theta)\cos(\phi)\Delta_{y_2}\right)e^{j\gamma_2} \\ \vdots \\ \left(-R\,\sin(\theta)\sin\left(\phi - \frac{2\pi(L-1)}{L}\right) - \sin(\theta)\sin(\phi)\Delta_{x_L} + \sin(\theta)\cos(\phi)\Delta_{y_L}\right)e^{j\gamma_L} \end{bmatrix},$$

$$\frac{\partial \boldsymbol{\mu}}{\partial \Delta} = \mathbf{s} \otimes \frac{\partial \mathbf{a}}{\partial \Delta} = j\frac{2\pi}{\lambda}\sigma_s \mathbf{s} \otimes \left[\sin(\theta)\cos(\phi),\ \sin(\theta)\sin(\phi),\ \cos(\theta)\right] \otimes \mathrm{diag}\left[e^{j\gamma_1}, e^{j\gamma_2}, \ldots, e^{j\gamma_L}\right].$$

b. Deriving $h_{i,j}$

Using Eq. (A6),

$$h_{\theta,\theta} = \frac{4M\sigma_s^2\pi^2}{\lambda^2}\sum_{\ell=1}^{L}\left\{\cos(\theta)\left[R\,\cos\left(\phi - \frac{2\pi(\ell-1)}{L}\right) + \cos(\phi)\Delta_{x_\ell} + \sin(\phi)\Delta_{y_\ell}\right] - \sin(\theta)\Delta_{z_\ell}\right\}^2,$$

$$h_{\theta,\phi} = \frac{4M\sigma_s^2\pi^2}{\lambda^2}\sum_{\ell=1}^{L}\left\{\cos(\theta)\left[R\,\cos\left(\phi - \frac{2\pi(\ell-1)}{L}\right) + \cos(\phi)\Delta_{x_\ell} + \sin(\phi)\Delta_{y_\ell}\right] - \sin(\theta)\Delta_{z_\ell}\right\}$$
$$\times\left[-R\,\sin(\theta)\sin\left(\phi - \frac{2\pi(\ell-1)}{L}\right) - \sin(\theta)\sin(\phi)\Delta_{x_\ell} + \sin(\theta)\cos(\phi)\Delta_{y_\ell}\right] = h_{\phi,\theta},$$

$$h_{\phi,\phi} = \frac{4M\sigma_s^2\pi^2}{\lambda^2}\sum_{\ell=1}^{L}\left[-R\,\sin(\theta)\sin\left(\phi - \frac{2\pi(\ell-1)}{L}\right) - \sin(\theta)\sin(\phi)\Delta_{x_\ell} + \sin(\theta)\cos(\phi)\Delta_{y_\ell}\right]^2,$$

$$\mathbf{h}_{\theta,\Delta} = \frac{4M\sigma_s^2\pi^2}{\lambda^2}\left[\sin(\theta)\cos(\phi),\ \sin(\theta)\sin(\phi),\ \cos(\theta)\right]$$
$$\otimes\begin{bmatrix} \left(R\,\cos(\theta)\cos(\phi) + \cos(\theta)\cos(\phi)\Delta_{x_1} + \cos(\theta)\sin(\phi)\Delta_{y_1} - \sin(\theta)\Delta_{z_1}\right) \\ \left(R\,\cos(\theta)\cos\left(\phi - \frac{2\pi}{L}\right) + \cos(\theta)\cos(\phi)\Delta_{x_2} + \cos(\theta)\sin(\phi)\Delta_{y_2} - \sin(\theta)\Delta_{z_2}\right) \\ \vdots \\ \left(R\,\cos(\theta)\cos\left(\phi - \frac{2\pi(L-1)}{L}\right) + \cos(\theta)\cos(\phi)\Delta_{x_L} + \cos(\theta)\sin(\phi)\Delta_{y_L} - \sin(\theta)\Delta_{z_L}\right) \end{bmatrix} = \mathbf{h}_{\Delta,\theta}^T,$$

$$\mathbf{h}_{\phi,\Delta} = \frac{4M\sigma_s^2\pi^2}{\lambda^2}\left[\sin(\theta)\cos(\phi),\ \sin(\theta)\sin(\phi),\ \cos(\theta)\right]$$
$$\otimes\begin{bmatrix} \left(-R\,\sin(\theta)\sin(\phi) - \sin(\theta)\sin(\phi)\Delta_{x_1} + \sin(\theta)\cos(\phi)\Delta_{y_1}\right) \\ \left(-R\,\sin(\theta)\sin\left(\phi - \frac{2\pi}{L}\right) - \sin(\theta)\sin(\phi)\Delta_{x_2} + \sin(\theta)\cos(\phi)\Delta_{y_2}\right) \\ \vdots \\ \left(-R\,\sin(\theta)\sin\left(\phi - \frac{2\pi(L-1)}{L}\right) - \sin(\theta)\sin(\phi)\Delta_{x_L} + \sin(\theta)\cos(\phi)\Delta_{y_L}\right) \end{bmatrix} = \mathbf{h}_{\Delta,\phi}^T,$$

$$\mathbf{h}_{\Delta,\Delta} = \frac{4M\sigma_s^2\pi^2}{\lambda^2}\begin{bmatrix} \sin^2(\theta)\cos^2(\phi) & \frac{1}{2}\sin^2(\theta)\sin(2\phi) & \frac{1}{2}\cos(\phi)\sin(2\theta) \\ \frac{1}{2}\sin^2(\theta)\sin(2\phi) & \sin^2(\theta)\sin^2(\phi) & \frac{1}{2}\sin(\phi)\sin(2\theta) \\ \frac{1}{2}\cos(\phi)\sin(2\theta) & \frac{1}{2}\sin(\phi)\sin(2\theta) & \cos^2(\theta) \end{bmatrix} \otimes \mathbf{I}_{L\times L}.$$

c. Obtaining the entries of J_D

Using Eq. (A6),

$$
\begin{aligned}
[\mathbf{J}_D]_{\theta,\theta} &= \frac{8M\sigma_s^2\pi^2}{\lambda^2\sigma_n^2}\sum_{\ell=1}^{L}E_\Delta\left\{\cos(\theta)\left[R\,\cos\left(\phi-\frac{2\pi(\ell-1)}{L}\right)+\cos(\phi)\Delta_{x_\ell}+\sin(\phi)\Delta_{y_\ell}\right]-\sin(\theta)\Delta_{z_\ell}\right\}^2\\
&= \frac{8M\sigma_s^2\pi^2}{\lambda^2\sigma_n^2}\sum_{\ell=1}^{L}\left\{\cos^2(\theta)\left[R^2\cos^2\left(\phi-\frac{2\pi(\ell-1)}{L}\right)+\sigma_{\Delta x}^2\cos^2(\phi)+\sigma_{\Delta y}^2\sin^2(\phi)\right]+\sigma_{\Delta z}^2\sin^2(\theta)\right\}\\
&= \frac{8M\sigma_s^2\pi^2}{\lambda^2\sigma_n^2}\left\{\cos^2(\theta)\left[R^2\underbrace{\sum_{\ell=1}^{L}\cos^2\left(\phi-\frac{2\pi(\ell-1)}{L}\right)}_{=L/2}+L\sigma_{\Delta x}^2\cos^2(\phi)+L\sigma_{\Delta y}^2\sin^2(\phi)\right]+L\sigma_{\Delta z}^2\sin^2(\theta)\right\}\\
&= \frac{4M\sigma_s^2L\pi^2}{\lambda^2\sigma_n^2}\left[R^2\cos^2(\theta)+2\sigma_{\Delta x}^2\cos^2(\theta)\cos^2(\phi)+2\sigma_{\Delta y}^2\cos^2(\theta)\sin^2(\phi)+2\sigma_{\Delta z}^2\sin^2(\theta)\right],\\
[\mathbf{J}_D]_{\theta,\phi} &= \frac{8M\sigma_s^2\pi^2}{\lambda^2\sigma_n^2}\sum_{\ell=1}^{L}E_\Delta\left\{\left[\cos(\theta)\left(R\,\cos\left(\phi-\frac{2\pi(\ell-1)}{L}\right)+\cos(\phi)\Delta_{x_\ell}+\sin(\phi)\Delta_{y_\ell}\right)-\sin(\theta)\Delta_{z_\ell}\right]\right.\\
&\quad\left.\times\left[-R\,\sin(\theta)\sin\left(\phi-\frac{2\pi(\ell-1)}{L}\right)-\sin(\theta)\sin(\phi)\Delta_{x_\ell}+\sin(\theta)\cos(\phi)\Delta_{y_\ell}\right]\right\}\\
&= -\frac{2M\sigma_s^2R^2\pi^2}{\lambda^2\sigma_n^2}\sin(2\theta)\underbrace{\sum_{\ell=1}^{L}\sin\left(2\phi-\frac{4\pi(\ell-1)}{L}\right)}_{=0}=0=[\mathbf{J}_D]_{\phi,\theta},\\
[\mathbf{J}_D]_{\phi,\phi} &= \frac{8M\sigma_s^2\pi^2}{\lambda^2\sigma_n^2}\sum_{\ell=1}^{L}E_\Delta\left[-R\,\sin(\theta)\sin\left(\phi-\frac{2\pi(\ell-1)}{L}\right)-\sin(\theta)\sin(\phi)\Delta_{x_\ell}+\sin(\theta)\cos(\phi)\Delta_{y_\ell}\right]^2\\
&= \frac{8M\sigma_s^2\pi^2}{\lambda^2\sigma_n^2}\sum_{\ell=1}^{L}\left[R^2\sin^2(\theta)\sin^2\right]\left(\phi-\frac{2\pi(\ell-1)}{L}\right)+\sigma_{\Delta x}^2\sin^2(\theta)\sin^2(\phi)+\sigma_{\Delta y}^2\sin^2(\theta)\cos^2(\phi)\\
&= \frac{8M\sigma_s^2\pi^2}{\lambda^2\sigma_n^2}\left[R^2\sin^2(\theta)\underbrace{\sum_{\ell=1}^{L}\sin^2\left(\phi-\frac{2\pi(\ell-1)}{L}\right)}_{=L/2}+L\sigma_{\Delta x}^2\sin^2(\theta)\sin^2(\phi)+L\sigma_{\Delta y}^2\sin^2(\theta)\cos^2(\phi)\right]\\
&= \frac{4M\sigma_s^2L\pi^2}{\lambda^2\sigma_n^2}\sin^2(\theta)\left[R^2+2\sigma_{\Delta x}^2\sin^2(\phi)+2\sigma_{\Delta y}^2\cos^2(\phi)\right],\\
[\mathbf{J}_D]_{\Delta,\Delta} &= 8M\left(\frac{\sigma_s\pi}{\lambda\sigma_n}\right)^2\begin{bmatrix}\sin^2(\theta)\cos^2(\phi) & \frac{1}{2}\sin^2(\theta)\sin(2\phi) & \frac{1}{2}\cos(\phi)\sin(2\theta)\\ \frac{1}{2}\sin^2(\theta)\sin(2\phi) & \sin^2(\theta)\sin^2(\phi) & \frac{1}{2}\sin(\phi)\sin(2\theta)\\ \frac{1}{2}\cos(\phi)\sin(2\theta) & \frac{1}{2}\sin(\phi)\sin(2\theta) & \cos^2(\theta)\end{bmatrix}\otimes\mathbf{I}_{L\times L},\\
[\mathbf{J}_D]_{\theta,\Delta} &= \frac{8M\sigma_s^2\pi^2}{\lambda^2\sigma_n^2}\left[\sin(\theta)\cos(\phi),\,\sin(\theta)\sin(\phi),\,\cos(\theta)\right]\\
&\quad\otimes E_\Delta\begin{bmatrix}\left(R\,\cos(\theta)\cos(\phi)+\cos(\theta)\cos(\phi)\Delta_{x_1}+\cos(\theta)\sin(\phi)\Delta_{y_1}-\sin(\theta)\Delta_{z_1}\right)\\ \left(R\,\cos(\theta)\cos\left(\phi-\frac{2\pi}{L}\right)+\cos(\theta)\cos(\phi)\Delta_{x_2}+\cos(\theta)\sin(\phi)\Delta_{y_2}-\sin(\theta)\Delta_{z_2}\right)\\ \vdots\\ \left(R\,\cos(\theta)\cos\left(\phi-\frac{2\pi(L-1)}{L}\right)+\cos(\theta)\cos(\phi)\Delta_{x_L}+\cos(\theta)\sin(\phi)\Delta_{y_L}-\sin(\theta)\Delta_{z_L}\right)\end{bmatrix}^T\\
&= \frac{8M\sigma_s^2R\pi^2}{\lambda^2\sigma_n^2}\left[\sin(\theta)\cos(\phi),\,\sin(\theta)\sin(\phi),\,\cos(\theta)\right]\\
&\quad\otimes\left[\cos(\theta)\cos(\phi),\,\cos(\theta)\cos(\phi-2\pi/L),\ldots,\,\cos(\theta)\cos\left(\phi-\frac{2\pi(L-1)}{L}\right)\right],
\end{aligned}
$$

$$[\mathbf{J}_D]_{\phi,\Delta} = \frac{8M\sigma_s^2\pi^2}{\lambda^2\sigma_n^2}\left[\sin(\theta)\cos(\phi),\ \sin(\theta)\sin(\phi),\ \cos(\theta)\right]$$
$$\otimes E_\Delta \begin{bmatrix} \left(-R\ \sin(\theta)\sin(\phi) - \sin(\theta)\sin(\phi)\Delta_{x_1} + \sin(\theta)\cos(\phi)\Delta_{y_1}\right) \\ \left(-R\ \sin(\theta)\sin(\phi - 2\pi/L) - \sin(\theta)\sin(\phi)\Delta_{x_2} + \sin(\theta)\cos(\phi)\Delta_{y_2}\right) \\ \vdots \\ \left(-R\ \sin(\theta)\sin\left(\phi - \frac{2\pi(L-1)}{L}\right) - \sin(\theta)\sin(\phi)\Delta_{x_L} + \sin(\theta)\cos(\phi)\Delta_{y_L}\right) \end{bmatrix}^T$$
$$= -\frac{8M\sigma_s^2R\pi^2}{\lambda^2\sigma_n^2}\left[\sin(\theta)\cos(\phi),\ \sin(\theta)\sin(\phi),\ \cos(\theta)\right]$$
$$\otimes \left[\sin(\theta)\sin(\phi),\ \sin(\theta)\sin(\phi - 2\pi/L), \ldots,\ \sin(\theta)\sin\left(\phi - \frac{2\pi(L-1)}{L}\right)\right],$$

$$[\mathbf{J}_B]_{\Delta,\Delta} := \frac{8M\sigma_s^2\pi^2}{\lambda^2\sigma_n^2}\begin{bmatrix} \sin^2(\theta)\cos^2(\phi) + \frac{\lambda^2\sigma_n^2}{8M\sigma_s^2\pi^2\sigma_{\Delta x}^2} & \frac{1}{2}\sin^2(\theta)\sin(2\phi) & \frac{1}{2}\cos(\phi)\sin(2\theta) \\ \frac{1}{2}\sin^2(\theta)\sin(2\phi) & \sin^2(\theta)\sin^2(\phi) + \frac{\lambda^2\sigma_n^2}{8M\sigma_s^2\pi^2\sigma_{\Delta y}^2} & \frac{1}{2}\sin(\phi)\sin(2\theta) \\ \frac{1}{2}\cos(\phi)\sin(2\theta) & \frac{1}{2}\sin(\phi)\sin(2\theta) & \cos^2(\theta) + \frac{\lambda^2\sigma_n^2}{8M\sigma_s^2\pi^2\sigma_{\Delta z}^2} \end{bmatrix} \otimes \mathbf{I}_{L\times L}. \tag{A7}$$

4. To express the HCRBs explicitly in terms of the data model parameters

Returning to Eq. (A1),

$$\mathbf{J}_B = \begin{bmatrix} \mathbf{G} & \mathbf{B} \\ \mathbf{B}^T & [\mathbf{J}_B]_{\Delta,\Delta} \end{bmatrix}, \tag{A8}$$

where $\boldsymbol{G}$ is defined in Eq. (A14), $[\mathbf{J}_B]_{\Delta,\Delta}$ is defined in Eq. (A7) and

$$\mathbf{B} := \left[\ [\mathbf{J}_D]_{\theta,\Delta} \quad [\mathbf{J}_D]_{\phi,\Delta}\ \right]^T \tag{A9}$$
$$= 8M\sigma_s^2R\left(\frac{\pi}{\lambda\sigma_n}\right)^2\left[\ \sin(\theta)\cos(\phi) \quad \sin(\theta)\sin(\phi) \quad \cos(\theta)\ \right] \otimes \begin{bmatrix} \cos(\theta)\cos(\phi), \ldots, & \cos(\theta)\cos\left(\phi - \frac{2\pi(L-1)}{L}\right) \\ -\sin(\theta)\sin(\phi), \ldots, & -\sin(\theta)\sin\left(\phi - \frac{2\pi(L-1)}{L}\right) \end{bmatrix}. \tag{A10}$$

Note that $\mathbf{G}$ is 2×2, $\mathbf{B}$ is $2\times 3L$, and $[\mathbf{J}_B]_{\Delta,\Delta}$ is $3L\times 3L$.

The HCRBs of θ and ϕ equal the first two diagonal entries of $\mathbf{J}_B^{-1}$. The 2×2 upper left submatrix of $\mathbf{J}_B^{-1}$ equals [see Eq. (2.3) on p. 120 of Ref. 66]

$$(\mathbf{G} - \mathbf{B}[\mathbf{J}_B]_{\Delta,\Delta}^{-1}\mathbf{B}^T)^{-1}, \tag{A11}$$

with

$$\mathbf{G} - \mathbf{B}[\mathbf{J}_B]_{\Delta,\Delta}^{-1}\mathbf{B}^T = M\sigma_s^2L\begin{bmatrix} \zeta_1 & 0 \\ 0 & \zeta_2 \end{bmatrix},$$

where ζ_1 and ζ_2 are defined in Eqs. (A15) and (A16), respectively.

These lead to the HCRBs of θ and ϕ as stated in Eqs. (3) and (4), respectively,

$$
\begin{aligned}
\mathbf{B}[\mathbf{J}_B]^{-1}_{\Delta,\Delta}\mathbf{B}^T = &\frac{8MR^2\sigma_s^2\pi^2}{\lambda^2\sigma_n^2}\begin{bmatrix}\sin(\theta)\cos(\phi) & \sin(\theta)\sin(\phi) & \cos(\theta)\end{bmatrix}\\
&\begin{bmatrix}
\sin^2(\theta)\cos^2(\phi)+\dfrac{\lambda^2\sigma_n^2}{8M\sigma_s^2\pi^2\sigma_{\Delta x}^2} & \dfrac{1}{2}\sin^2(\theta)\sin(2\phi) & \dfrac{1}{2}\cos(\phi)\sin(2\theta)\\
\dfrac{1}{2}\sin^2(\theta)\sin(2\phi) & \sin^2(\theta)\sin^2(\phi)+\dfrac{\lambda^2\sigma_n^2}{8M\sigma_s^2\pi^2\sigma_{\Delta y}^2} & \dfrac{1}{2}\sin(\phi)\sin(2\theta)\\
\dfrac{1}{2}\cos(\phi)\sin(2\theta) & \dfrac{1}{2}\sin(\phi)\sin(2\theta) & \cos^2(\theta)+\dfrac{\lambda^2\sigma_n^2}{8M\sigma_s^2\pi^2\sigma_{\Delta z}^2}
\end{bmatrix}^{-1}\\
&\begin{bmatrix}\sin(\theta)\cos(\phi) & \sin(\theta)\sin(\phi) & \cos(\theta)\end{bmatrix}^T\otimes
\begin{bmatrix}
\cos(\theta)\left(\cos(\phi),\ldots,\cos\left(\phi-\dfrac{2\pi(L-1)}{L}\right)\right)\\
\sin(\theta)\left(-\sin(\phi),\ldots,-\sin\left(\phi-\dfrac{2\pi(L-1)}{L}\right)\right)
\end{bmatrix}\\
&\begin{bmatrix}
\cos(\theta)\cos(\phi) & -\sin(\theta)\sin(\phi)\\
\cos(\theta)\cos\left(\phi-\dfrac{2\pi}{L}\right) & -\sin(\theta)\sin\left(\phi-\dfrac{2\pi}{L}\right)\\
\vdots & \vdots\\
\cos(\theta)\cos\left(\phi-\dfrac{2\pi(L-1)}{L}\right) & -\sin(\theta)\sin\left(\phi-\dfrac{2\pi(L-1)}{L}\right)
\end{bmatrix}\\
=&\frac{8MR^2\sigma_s^2\pi^2}{\lambda^2\sigma_n^2}\begin{bmatrix}\sin(\theta)\cos(\phi) & \sin(\theta)\sin(\phi) & \cos(\theta)\end{bmatrix}^T\\
&\begin{bmatrix}
\sin^2(\theta)\cos^2(\phi)+\dfrac{\lambda^2\sigma_n^2}{8M\sigma_s^2\pi^2\sigma_{\Delta x}^2} & \dfrac{1}{2}\sin^2(\theta)\sin(2\phi) & \dfrac{1}{2}\cos(\phi)\sin(2\theta)\\
\dfrac{1}{2}\sin^2(\theta)\sin(2\phi) & \sin^2(\theta)\sin^2(\phi)+\dfrac{\lambda^2\sigma_n^2}{8M\sigma_s^2\pi^2\sigma_{\Delta y}^2} & \dfrac{1}{2}\sin(\phi)\sin(2\theta)\\
\dfrac{1}{2}\cos(\phi)\sin(2\theta) & \dfrac{1}{2}\sin(\phi)\sin(2\theta) & \cos^2(\theta)+\dfrac{\lambda^2\sigma_n^2}{8M\sigma_s^2\pi^2\sigma_{\Delta z}^2}
\end{bmatrix}^{-1}\\
&\begin{bmatrix}\sin(\theta)\cos(\phi)\\ \sin(\theta)\sin(\phi)\\ \cos(\theta)\end{bmatrix}\otimes
\begin{bmatrix}
\cos^2(\theta)\underbrace{\sum_{\ell=1}^{L}\cos^2\left(\phi-\dfrac{2\pi(L-1)}{L}\right)}_{=\frac{L}{2}} & -\dfrac{\sin(2\theta)}{2}\underbrace{\sum_{\ell=1}^{L}\sin\left(2\phi-\dfrac{4\pi(L-1)}{L}\right)}_{=0}\\
-\dfrac{\sin(2\theta)}{2}\sum_{\ell=1}^{L}\sin\left(2\phi-\dfrac{4\pi(L-1)}{L}\right) & \sin^2(\theta)\underbrace{\sum_{\ell=1}^{L}\sin^2\left(\phi-\dfrac{2\pi(L-1)}{L}\right)}_{=\frac{L}{2}}
\end{bmatrix}
\end{aligned}
\tag{A12}
$$

$$
=\frac{4ML\sigma_s^2\pi^2}{\lambda^2\sigma_n^2}\frac{\sin^2(\theta)\left[\sigma_{\Delta x}^2\cos^2(\phi)+\sigma_{\Delta y}^2\sin^2(\phi)\right]+\sigma_{\Delta z}^2\cos^2(\theta)}{\sin^2(\theta)\left[\sigma_{\Delta x}^2\cos^2(\phi)+\sigma_{\Delta y}^2\sin^2(\phi)\right]+\sigma_{\Delta z}^2\cos^2(\theta)+\dfrac{\lambda^2\sigma_n^2}{8M\sigma_s^2\pi^2}}\begin{bmatrix}R^2\cos^2(\theta) & 0\\ 0 & R^2\sin^2(\theta)\end{bmatrix},
\tag{A13}
$$

$$
\begin{aligned}
\mathbf{G}:=&\begin{bmatrix}[\mathbf{J}_D]_{\theta,\theta} & [\mathbf{J}_D]_{\theta,\phi}\\ [\mathbf{J}_D]_{\phi,\theta} & [\mathbf{J}_D]_{\phi,\phi}\end{bmatrix}\\
=&\frac{4ML\sigma_s^2\pi^2}{\lambda^2\sigma_n^2}\begin{bmatrix}
\cos^2(\theta)\left\{R^2+2\sigma_{\Delta x}^2\cos^2(\phi)+2\sigma_{\Delta y}^2\sin^2(\phi)+2\sigma_{\Delta z}^2\sin^2(\theta)\right\} & 0\\
0 & \sin^2(\theta)\left\{R^2+2\sigma_{\Delta x}^2\sin^2(\phi)+2\sigma_{\Delta y}^2\cos^2(\phi)\right\}
\end{bmatrix},
\end{aligned}
\tag{A14}
$$

$$\zeta_1 = \left(\frac{2\pi}{\lambda\sigma_n}\right)^2 \left(\cos^2(\theta)\left[R^2 + 2\sigma_{\Delta x}^2\cos^2\phi + 2\sigma_{\Delta y}^2\sin^2(\phi)\right] + 2\sigma_{\Delta z}^2\sin^2(\theta) \right.$$
$$\left. - \frac{R^2\cos^2(\theta)\left\{\sin^2(\theta)\left[\sigma_{\Delta x}^2\cos^2(\phi) + \sigma_{\Delta y}^2\sin^2(\phi)\right] + \sigma_{\Delta z}^2\cos^2\theta\right\}}{\sin^2(\theta)\left[\sigma_{\Delta x}^2\cos^2(\phi) + \sigma_{\Delta y}^2\sin^2(\phi)\right] + \sigma_{\Delta z}^2\cos^2(\theta) + \frac{\lambda^2\sigma_n^2}{8M\sigma_s^2\pi^2}} \right)$$
$$= 2\left(\frac{2\pi}{\sigma_n}\right)^2 \left\{ \cos^2(\theta)\left[\frac{\sigma_{\Delta x}^2}{\lambda^2}\cos^2(\phi) + \frac{\sigma_{\Delta y}^2}{\lambda^2}\sin^2(\phi)\right] + \sigma_{\Delta z}^2\sin^2(\theta) \right\}$$
$$+ \frac{(R/\lambda)^2\cos^2(\theta)}{\left(\frac{\sigma_n}{2\pi}\right)^2 + 2M\sigma_s^2\left\{ \sin^2(\theta)\left[\frac{\sigma_{\Delta x}^2}{\lambda^2}\cos^2(\phi) + \frac{\sigma_{\Delta y}^2}{\lambda^2}\sin^2(\phi)\right] + \frac{\sigma_{\Delta z}^2}{\lambda^2}\cos^2(\theta) \right\}}, \tag{A15}$$

$$\zeta_2 = \left(\frac{2\pi}{\lambda\sigma_n}\right)^2 \left(\sin^2(\theta)\left[R^2 + 2\sigma_{\Delta x}^2\sin^2(\phi) + 2\sigma_{\Delta y}^2\cos^2(\phi)\right] \right.$$
$$\left. - \frac{R^2\sin^2(\theta)\left\{\sin^2(\theta)\left[\sigma_{\Delta x}^2\cos^2(\phi) + \sigma_{\Delta y}^2\sin^2(\phi)\right] + \sigma_{\Delta z}^2\cos^2(\theta)\right\}}{\sin^2(\theta)\left[\sigma_{\Delta x}^2\cos^2(\phi) + \sigma_{\Delta y}^2\sin^2(\phi)\right] + \sigma_{\Delta z}^2\cos^2(\theta) + \frac{\lambda^2\sigma_n^2}{8M\sigma_s^2\pi^2}} \right)$$
$$= 2\left(\frac{2\pi\sin(\theta)}{\sigma_n}\right)^2 \left[\frac{\sigma_{\Delta x}^2}{\lambda^2}\sin^2(\phi) + \frac{\sigma_{\Delta y}^2}{\lambda^2}\cos^2(\phi)\right]$$
$$+ \frac{(R/\lambda)^2\sin^2(\theta)}{\left(\frac{\sigma_n}{2\pi}\right)^2 + 2M\sigma_s^2\left\{ \sin^2(\theta)\left[\frac{\sigma_{\Delta x}^2}{\lambda^2}\cos^2(\phi) + \frac{\sigma_{\Delta y}^2}{\lambda^2}\sin^2(\phi)\right] + \frac{\sigma_{\Delta z}^2}{\lambda^2}\cos^2\theta \right\}}. \tag{A16}$$

[1]This is a commercial product "xCORE VocalFusion™ Speaker Part Number XK-VF3100-C43" manufactured by *XMOS* (Bristol, UK).
[2]Equipment, available at https://www.smard.es.aau.dk/equipment/ (Last viewed 15 September 2018).
[3]This is a commercial product "UMA-8" manufactured by *miniDSP* (Hong Kong, China).
[4]"UMA-8-SP, user manual," available at https://www.minidsp.com/products/usb-audio-interface/uma-8-sp-detail (Last viewed 15 September 2018).
[5]H. Teutsch and W. Kellermann, "Acoustic source detection and localization based on wavefield decomposition using circular microphone arrays," J. Acoust. Soc. Am. **120**(5), 2724–2736 (2006).
[6]E. Tiana-Roig, F. Jacobsen, and E. F. Grande, "Beamforming with a circular microphone array for localization of environmental noise sources," J. Acoust. Soc. Am. **128**(6), 3535–3542 (2010).
[7]S. Yan, "Optimal design of modal beamformers for circular arrays," J. Acoust. Soc. Am. **138**(4), 2140–2151 (2015).
[8]A. Parthy, N. Epain, A. V. Schaik, and C. T. Jin, "Comparison of the measured and theoretical performance of a broadband circular microphone array," J. Acoust. Soc. Am. **130**(6), 3827–3837 (2011).
[9]M. R. Bai, C.-S. Lai, and P.-C. Wu, "Localization and separation of acoustic sources by using a 2.5-dimensional circular microphone array," J. Acoust. Soc. Am. **142**(1), 286–297 (2017).
[10]H. R. Karimi and A. Manikas, "Manifold of a planar array and its effects on the accuracy of direction-finding systems," IEE Proc. Radar, Sonar Navig. **143**(6), 349–357 (1996).
[11]H. Gazzah and S. Marcos, "Antenna arrays for enhanced estimation of azimuth and elevation," in *IEEE International Conference on Acoustics, Speech and Signal Processing* (2003), pp. v213–v216.
[12]F. Bellili, S. Affes, and A. Stéphenne, "On the lower performance bounds for DOA estimators from linearly-modulated signals," in *Biennial Symposium on Communications* (2010), pp. 381–386.
[13]W. Yao and C. Hui, "Performance analysis of two kinds of uniform circular arrays," in *International Conference on Multimedia and Signal Processing* (2011), Vol. 2, pp. 52–56.
[14]J. P. Delmas and H. Gazzah, "CRB analysis of near-field source localization using uniform circular arrays," in *IEEE International Conference on Acoustics, Speech and Signal Processing* (2013), pp. 3996–4000.
[15]D. M. Kitavi, T.-C. Lin, K. T. Wong, and Y. I. Wu, "Direction finding with the sensors' gains suffering Bayesian uncertainty–hybrid CRB and MAP estimation," IEEE Trans. Aerospace Electron. Syst. **52**(4), 2038–2044 (2016).
[16]J. P. Delmas, M. N. El Korso, H. Gazzah, and M. Castella, "CRB analysis of planar antenna arrays for optimizing near-field source localization," Signal Process. **127**, 117–134 (2016).
[17]B. Friedlander and A. J. Weiss, "Direction finding in the presence of mutual coupling," IEEE Trans. Antennas Propag. **39**(3), 273–284 (1991).
[18]C. P. Mathews and M. D. Zoltowski, "Eigenstructure techniques for 2-D angle estimation with uniform circular arrays," IEEE Trans. Signal Process. **42**(9), 2395–2407 (1994).

[19]A. Y. J. Chan and J. Litva, "MUSIC and maximum likelihood techniques on two-dimensional DOA estimation with uniform circular array," IEE Proc. Radar, Sonar Navig. **142**(3), 105–114 (1995).
[20]J. Sheinvald, M. Wax, and A. J. Weiss, "On the achievable localization accuracy of multiple sources at high SNR," IEEE Trans. Signal Process. **45**(7), 1795–1799 (1997).
[21]C. W. Ang, C. M. See, and A. C. Kot, "Optimization of array geometry for identifiable high resolution parameter estimation in sensor array signal processing," in *International Conference on Information, Communications and Signal Processing* (1997), pp. 1613–1617.
[22]O. Birkenes, R. A. Kennedy, and T. S. Pollock, "Spatial limits for direction of arrival estimation for narrowband wireless communication," in *Norwegian Signal Processing Symposium* (2003).
[23]J. Tao, Y. Shi, and W. Chang, "Estimation of azimuth-elevation on non-ideal UCA," in *Sensor Array and Multichannel Signal Processing Workshop* (2004), pp. 580–583.
[24]J. Tao, J. Tao, and H. Xu, "Simple and accurate DOA estimator with UCA in multiplicative noise environments," in *International Conference on Radar* (2006).
[25]C. Park and D. Kim, "The fast correlative interferometer direction finder using I/Q demodulator," in *Asia-Pacific Conference on Communications* (2006).
[26]M. Akcakaya, C. H. Muravchik, and A. Nehorai, "Biologically inspired coupled antenna array for direction of arrival estimation," IEEE Trans. Signal Process. **59**(10), 4795–4808 (2011).
[27]B. R. Jackson, S. Rajan, B. J. Liao, and S. Wang, "Direction of arrival estimation using directive antennas in uniform circular arrays," IEEE Trans. Antennas Propag. **63**(2), 736–747 (2015).
[28]M. D. Zoltowski and C. P. Mathews, "Closed-form 2D angle estimation with uniform circular arrays via phase mode excitation and ESPRIT," in *Asilomar Conference on Signals, Systems and Computers* (1993), Vol. 1, pp. 169–173.
[29]C. P. Mathews and M. D. Zoltowski, "Performance analysis of the UCA-ESPRIT algorithm for circular ring arrays," IEEE Trans. Signal Process. **42**(9), 2535–2539 (1994).
[30]B. P. Flanagan and K. L. Bell, "Array self calibration with large sensor position errors," in *Asilomar Conference on Signals, Systems and Computers* (1999), pp. 258–262.
[31]B. P. Flanagan and K. L. Bell, "Improved array self calibration with large sensor position errors for closely spaced sources," in *IEEE Sensor Array and Multichannel Signal Processing Workshop* (2000), pp. 484–488.
[32]J.-J. Fuchs, "On the application of the global matched filter to DOA estimation with uniform circular arrays," IEEE Trans. Signal Process. **49**(4), 702–709 (2001).
[33]B. P. Flanagan and K. L. Bell, "Array self-calibration with large sensor position errors," Signal Process. **81**(10), 2201–2214 (2001).
[34]J. Lee, I. Song, and J. G. Joung, "Uniform circular array in the parameter estimation of coherently distributed sources," in *IEEE Military Communications Conference* (2002), Vol. 2, pp. 1258–1262.
[35]M. Pesavento and J. F. Böhme, "Direction of arrival estimation in uniform circular arrays composed of directional elements," in *IEEE Sensor Array and Multichannel Signal Processing Workshop* (2002), pp. 503–507.
[36]J. Lee, I. Song, H. Kwon, and S. R. Lee, "Low-complexity estimation of 2D DOA for coherently distributed sources," Signal Process. **83**, 1789–1802 (2003).
[37]F. Belloni and V. Koivunen, "Unitary root-MUSIC technique for uniform circular array," in *IEEE International Symposium on Signal Processing and Information Technology* (2004), pp. 451–454.
[38]C. Qi, Y. Wang, Y. Zhang, and H. Chen, "DOA estimation and self-calibration algorithm for uniform circular array," Electron. Lett. **41**(20), 1092–1093 (2005).
[39]F. Belloni, A. Richter, and V. Koivunen, "Reducing excess variance in beamspace methods for uniform circular array," in *IEEE Workshop on Statistical Signal Processing* (2005), pp. 940–943.
[40]F. Belloni and V. Koivunen, "Reducing bias in beamspace methods for uniform circular array," in *IEEE International Conference on Acoustics, Speech, and Signal Processing* (2005), Vol. 4, pp. 973–976.
[41]M. I. Y. Williams, G. Dickins, R. A. Kennedy, and T. D. Abhayapala, "Spatial limits on the performance of direction of arrival estimation," in *6th Australian Communications Theory Workshop* (2005), pp. 189–194.
[42]F. Belloni and V. Koivunen, "Beamspace transform for UCA: Error analysis and bias reduction," IEEE Trans. Signal Process. **54**(8), 3078–3089 (2006).
[43]M. Lin and L. Yang, "Blind calibration and DOA estimation with uniform circular arrays in the presence of mutual coupling," IEEE Antennas Wireless Propag. Lett. **5**(1), 315–318 (2006).
[44]R. Goossens and H. Rogier, "Estimation of direction-of-arrival and polarization with diversely polarized antennas in a circular symmetry incorporating mutual coupling effects," in *European Conference on Antennas and Propagation* (2006).
[45]R. Goossens and H. Rogier, "A hybrid UCA-RARE/root-MUSIC approach for 2-D direction of arrival estimation in uniform circular arrays in the presence of mutual coupling," Trans. Antennas Propag. **55**(3), 841–849 (2007).
[46]R. Goossens and H. Rogier, "2-D direction-of-arrival estimation in the presence of mutual coupling by exploiting the symmetry in a uniform circular array," in *IEEE Antennas and Propagation Society International Symposium* (2007), pp. 5283–5286.
[47]Z. Xiaofei, S. Ying, Z. Ruina, L. Wen, and X. Dazhuan, "Blind 2D-DOA estimation for uniform circular array," in *IEEE International Symposium on Microwave, Antenna, Propagation, and EMC Technologies For Wireless Communications* (2007), pp. 589–592.
[48]C. Zhang, K. Chen, and S. Yan, "A DOA estimation algorithm of acoustic sources based on wavefield decomposition using UCAs," in *International Conference on Communications and Networking in China* (2007), pp. 659–663.
[49]R. Goossens and H. Rogier, "Direction-of-arrival and polarization estimation with uniform circular arrays in the presence of mutual coupling," AEU Int. J. Electron. Commun. **62**(3), 199–206 (2008).
[50]Y. Wu and H. C. So, "Simple and accurate two-dimensional angle estimation for a single source with uniform circular array," IEEE Antennas Wireless Propag. Lett. **7**, 78–80 (2008).
[51]R. Goossens, H. Rogier, and S. Werbrouck, "UCA root-MUSIC with sparse uniform circular arrays," IEEE Trans. Signal Process. **56**(8), 4095–4099 (2008).
[52]T. E. Tuncer and M. T. Ozgen, "No-search algorithm for direction of arrival estimation," Radio Sci. **44**(RS5007), 1–14, https://doi.org/10.1029/2009RS004164 (2009).
[53]J. Pan and J. Zhou, "Beamspace PM-root-MUSIC for uniform circular array based on MST," in *International Joint Conference on Computational Sciences and Optimization* (2009), pp. 899–901.
[54]B. H. Wang, H. T. Hui, and M. S. Leong, "Decoupled 2D direction of arrival estimation using compact uniform circular arrays in the presence of elevation-dependent mutual coupling," Trans. Antennas Propag. **58**(3), 747–755 (2010).
[55]Z. Hu, F. He, and J. Zhu, "Blind source separation-based 2-D angle estimation with uniform circular array," in *IEEE International Conference on Wireless Communications and Signal Processing* (2010).
[56]J. Xie, Z. He, H. Li, and J. Li, "2D DOA estimation with sparse uniform circular arrays in the presence of mutual coupling," EURASIP J. Adv. Signal Process. **2011**, 127.
[57]J. L. Xie, Z. S. He, and H. Y. Li, "A fast DOA estimation algorithm for uniform circular arrays in the presence of unknown mutual coupling," Prog. Electromagn. Res. C **21**, 257–271 (2011).
[58]W. Tidd, Y. Zhao, and Y. Huang, "A compact beamspace DOA estimation and beamforming communication device," in *Aerospace Conference* (2011), pp. 1–8.
[59]B. Liao, Y. T. Wu, and S. C. Chan, "A generalized algorithm for fast two-dimensional angle estimation of a single source with uniform circular arrays," IEEE Antennas Wireless Propag. Lett. **11**, 984–986 (2012).
[60]T. J. Jung and K. Lee, "Closed-form algorithm for 3-D single-source localization with uniform circular array," IEEE Antennas Wireless Propag. Lett. **13**, 1096–1099 (2014).
[61]T. E. Tuncer and B. Friedlander, *Classical and Modern Direction-of-Arrival Estimation* (Academic, Burlington, MA, 2009).
[62]A necessary and sufficient condition for the HCRB to equal the CRB is given in Eq. (34) of Ref. 64.
[63]This case has been graphically investigated in Refs. 30, 31, and 33, which do not derive any Cramér-Rao bound in any detail, nor state any mathematical expression of any Cramér-Rao bound. Hence, Eqs. (11) and (12) here are new to the open literature, to the best of the present authors' knowledge.
[64]Y. Noam and H. Messer, "Notes on the tightness of the hybrid Cramér-Rao lower bound," IEEE Trans. Signal Process. **57**(6), 2074–2084 (2009).
[65]H. L. Van Trees, *Optimum Array Processing: Part IV of Detection, Estimation and Modulation Theory* (Wiley, New York, 2002).
[66]T. T. Lu and S. H. Shiou, "Inverses of 2×2 block matrices," Comput. Math. Appl. **43**, 119–129 (2002).
[67]"VocalFusion Speaker Product Brief," available at http://www.xmos.com/tw/support/boards?product=35855 (Last viewed 15 September 2018).